IEEE Access
Multidisciplinary | Rapid Review | Open Access Journal

Received April 24, 2019, accepted May 18, 2019, date of publication May 27, 2019, date of current version June 10, 2019.

Digital Object Identifier 10.1109/ACCESS.2019.2919238

Open-Circuit Switch-Fault Tolerant Control of a Modified Boost DC–DC Converter for Alternative Energy Systems

TAEHYUNG KIM[1], (Senior Member, IEEE), HYUNG-WOO LEE[2], (Member, IEEE), AND SANGSHIN KWAK[3], (Member, IEEE)

[1]Electrical and Computer Engineering Department, University of Michigan-Dearborn, Dearborn, MI 48128, USA
[2]Railway Vehicle System Engineering Department, Korea National University of Transportation, Uiwang-si 16106, South Korea
[3]School of Electrical and Electronics Engineering, Chung-Ang University, Seoul 06974, South Korea

Corresponding author: Taehyung Kim (taehyung@umich.edu)

This work was supported by the Mcubed, University of Michigan, under Grant U064054.

ABSTRACT This paper presents switch fault detection and compensation control schemes for a modified dc–dc converter that relocates a diode location. The proposed fault detection and compensation control schemes are applicable to various energy generation systems that include energy storage. A fault detection index has been introduced to detect an open switch fault in the modified converter structure, and a compensation control method based on a mixed switching strategy has been developed. The fault-tolerant control method along with the detection scheme can make a system return to work even under a switch fault. The proposed schemes have been tested and verified both by the simulations and by experiments using a TMS320F28335 DSP. The results will significantly improve the reliability of alternative energy generation systems against open switch faults.

INDEX TERMS Open switch fault, dc-dc converter, fault detection.

I. INTRODUCTION

The demand for alternative energy harvesting systems has been steadily increasing recently [1], [2]. Traditional power generation using fossil fuels pollutes the environment and affects the earth's temperature [1], [2], [4], [5].

It is well known that sustainable energy sources can eliminate harmful emissions and be inexhaustible resources to generate electricity [1]–[8]. Therefore, significant efforts have been devoted to developing alternative energy generation systems such as photovoltaics, wind, and fuel cells [1]–[15]. However, unpredictable power generation especially for photovoltaics and wind turbines, is a disadvantage of renewable energy systems. Therefore, energy storage (battery or ultracapacitor) is included in many such systems [4], [5], [8]–[10].

Since multiple high-frequency switching elements are employed for alternative energy systems, the demand for reliable energy conversion systems is rising. In many countries, offshore wind farms are constructed due to the higher wind energy in the ocean on the continental shelf [3], [4], [6]. Each unit has an energy conversion system based on power electronics technology.

If even a minor fault occurs in a wind turbine unit by just one switch failure, the wind farm system controller will simply shut down the unit and demand more power from other units to compensate for the fault and manage the wind farm. Repairing the unit's switch fault takes a much longer time for offshore wind farms, and if there is no fault detection logic in the unit, more delay will be expected.

In this paper, fault detection and compensation techniques have been researched for an open switch fault in a modified dc-dc converter that relocates a diode location.

These techniques will make a power conversion system work continuously even after a switch fault occurrence. Having this feature in place, the system will continue operating until engineers, knowing the fault location, can access the system to fix it. Switch fault detection and compensation have been an important research topic to improve the reliability of power conversion systems [15]–[24]. Although the majority of fault detection and compensation research has been done on ac-dc, dc-ac, and ac-ac converters, there

The associate editor coordinating the review of this manuscript and approving it for publication was Sing Kiong Nguang.

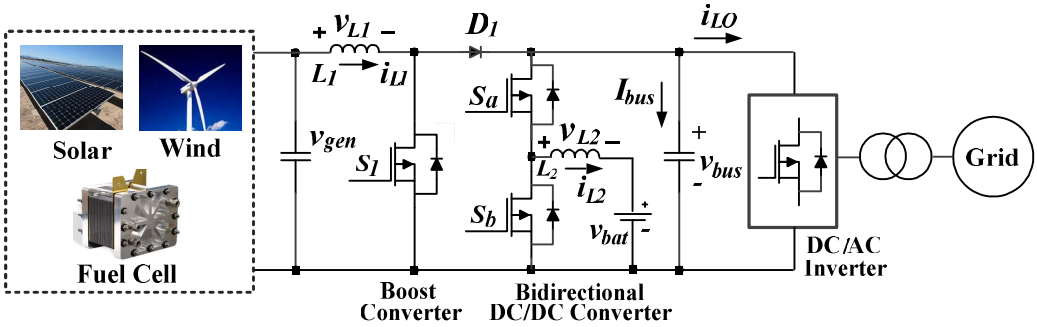

FIGURE 1. Power conversion system structure with an energy storage for alternative energy systems.

have been research efforts focused on the dc-dc converter side [17]–[24].

In [17], a magnetic near field waveform is used based on magnetic probes to diagnose switch faults. By the fast Fourier transformation, the frequency components of the waveforms are extracted to create a switch fault signal. The costly magnetic probes and high processing time and complexity are the main disadvantages of the method. In [18], inductor current slopes are utilized to monitor switch fault detection of non-isolated dc-dc converters. A diode voltage is measured in [19] as the fault detection signature to monitor both switch and diode faults. In [20], a stochastic fault diagnosis, rather than deterministic systems using Kalman filters, is reported for a boost dc-dc converter.

Ribeiro *et al.* [21] propose an open-circuit fault detection using the DC-link current derivative based on its sign variation during different time intervals. These approaches in [17]–[21] propose switch fault detection and monitoring methods without compensation schemes for dc-dc converters.

Various fault compensation methods along with detection schemes for dc-dc converters are reported [16], [22]–[24]. However, for an open-circuit fault of the main switch in a non-isolated boost dc-dc converter, there has been no ultimate solution to deliver power to the output boosting the DC-bus

voltage except for methods based on a redundant switch [16], [23]–[24].

The proposed fault detection and compensation concept has been developed for a system that includes energy storage with charging/discharging power flows having a total of three switches (one for voltage boosting and two for charging/discharging of the energy storage). In [24], a redundant switch is dedicated to the replacement of a faulty switch. For normal operation, the redundant switch does not operate. However, in our circuits, all three switches are operating during normal conditions for the boosting and charging/discharging operations. Therefore, we consider that there is no redundant switch in the proposed system.

The proposed technique can be applied to various application areas including alternative energy harvesting systems, such as solar, wind and fuel cell generation systems.

In section II, the proposed switch fault detection and compensation schemes are explained in detail using a modified boost converter structure. The compensation control strategies for both charging and discharging modes are presented as well. In section III, the proposed approaches are verified both by simulations and by experiments. For experiments, a prototype test bed with a Texas Instruments 32-bit DSP has been used.

II. PRINCIPLE OF FAULT DETECTION AND COMPENSATION

A power conversion system structure with a battery for alternative energy sources is presented in Figure 1. The two-stage converter (boost + bi-directional dc-dc converters) structure with energy storage can be applied to renewable energy generation systems to store energy for cases when the input source cannot provide sufficient energy.

The input source cannot supply power to the output side if an open-circuit switch fault occurs in the main switch (S_1) and the DC-bus voltage can decrease down to the input voltage level. This lower DC-bus voltage influences the inverter operation, and the system cannot supply the desired power to the load.

An extra switch connected in series for a short fault and in parallel for an open fault will be a simple solution for the S_1 switch. If there is no redundant switch, the structure in Figure 1 needs to be slightly modified to add a fault-tolerant characteristic. Figure 2 illustrates a modified structure where the D_1diode is relocated.

The structure in Figure 2 was created based on our research group's previous work on multi-functional converter circuits [9]. In [9], a converter structure with a relocated diode (using only two switches) was introduced to save cost. In this paper, the modified circuit structure employs three switches with standard control strategies and a fault detection and compensation algorithm is developed.

Under the open switch fault, the proposed compensation control utilizes the S_a and S_b switches to make the system still boost the input voltage and supply power to the output from the input source. In Figure 2, the D_1 diode is relocated close to the bus capacitor to use the S_a and S_b switches in the case of an S_1 switch fault. Under normal conditions, two switches (S_a and S_b) are controlled to charge/discharge an energy storage device (battery).

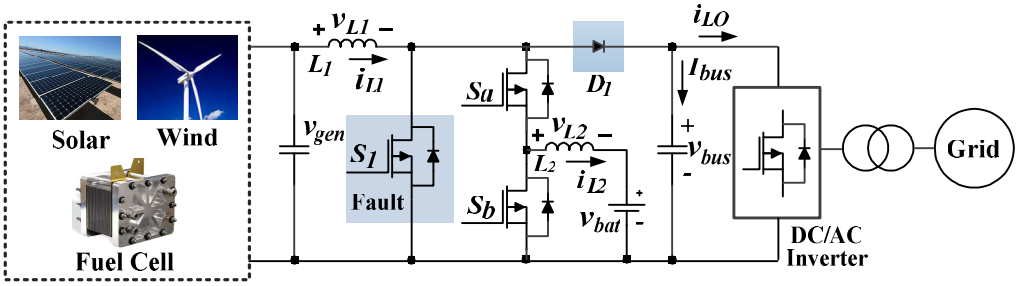

FIGURE 2. Modified power conversion system structure with an energy storage.

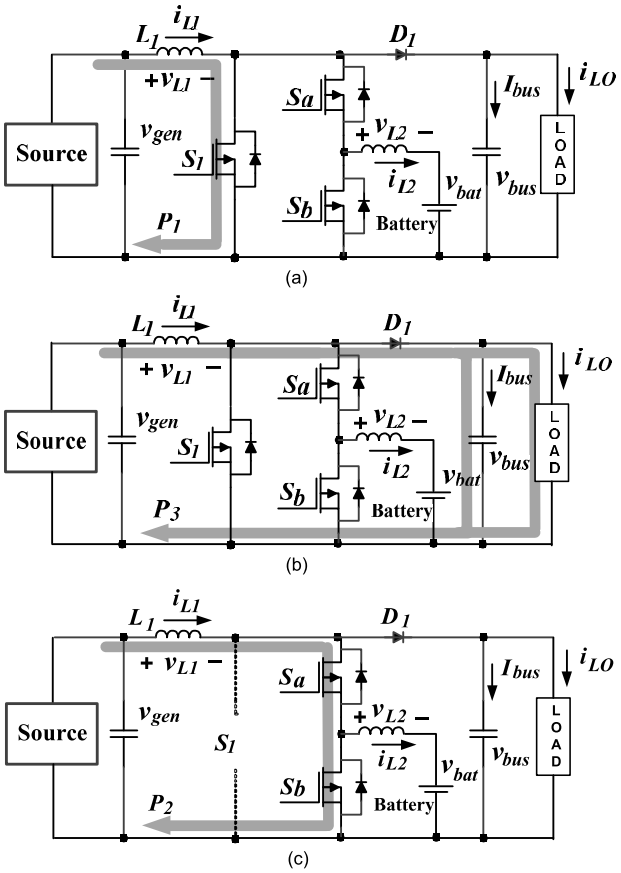

FIGURE 3. Current paths of the boost converter. (a) During S_1 being on (without a switch fault). (b) During S_1 being off (without a switch fault). (c) Alternative current path under S_1 switch fault (open fault).

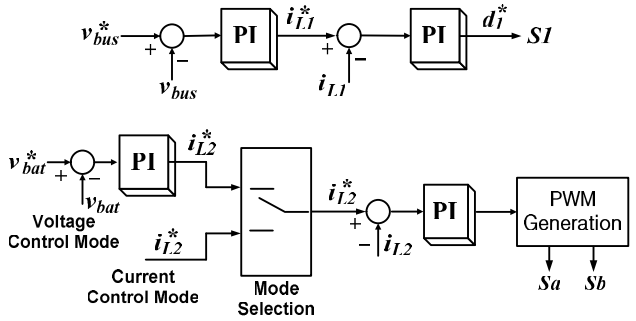

FIGURE 4. Control structure for normal operations (without any switch fault).

If an S_1 switch fault occurs, the S_a and S_b switches will have the functionality to activate both the boost converter and the bi-directional converter at the same time based on a fault compensation control strategy.

During normal operation, S_1 is on (Figure 3 (a)) to increase the inductor energy. Figure 3(b) illustrates the circuit behavior to supply power from the wind turbine and inductor to the output side (P_3) when the S_1 switch is off.

If a switch fault occurs in the S_1 switch, the P_1 current path in Figure 3(a) is disabled. Then, S_a and S_b switches will be turned on simultaneously to create an alternative current path (P_2) to increase the energy of the main inductor as depicted in Figure 3(c). For the P3 current flow in Figure 3(b), both S_a and S_b switches will be turned off to supply power from the wind turbine and the stored energy in the main inductor (L_1). In this way, the voltage boosting can be continued regardless of the S_1 switch fault. To boost and charge a battery at the same time, the S_a on period should be extended (S_b is off) after the P_2 current conduction. In contrast, to boost and discharge a battery simultaneously, the S_b on period needs to be extended (S_a is off) after the P_2 current conduction.

A. SWITCH FAULT DETECTION SCHEME

Figure 4 presents a control structure for a normal operation without any switch fault based on the structure in Figure 2. In this case, the boost converter (with S_1 switch) and the bi-directional dc-dc converter (with S_a and S_b switches) are independently controlled using PI controllers. For the bi-directional converter, a voltage control mode is mostly used to regulate the voltage level. However, for battery charging, a current control mode can be used for the constant-current charging mode, typically at the beginning of battery charging [25].

If the S_1 switch has an open fault, the main inductor current i_{L1} decreases to zero until the DC-bus voltage decreases below the input voltage. During this period, the main inductor current command (i^*_{L1}) which is the output of the voltage PI controller will increase since the measured voltage decreases.

To detect the S_1 switch fault, a fault detection index (FD_{idx}) is created as (1). The fault detection index is a ratio between

the inductor current command (i^*_{L1}) and the sum of the measured inductor current (i_{L1}) and the load current (i_{LO}).

$$FD_{idx} = \frac{i^*_{L1}}{i_{L1} + i_{LO}} \tag{1}$$

As illustrated in Figure 4, a dual-loop control structure with voltage and current controllers is used to control the DC-bus voltage. If the S_1 switch fails, the P_1 current path in Figure 3(a) will be disabled. This will cause a sudden inductor current (i_{L1}) and an output voltage, v_{bus} drop. Then, as aforementioned the output voltage controller will suddenly raise the current command of the main inductor (i^*_{L1}) since the measured output voltage will keep on falling. As a result, the fault detection index (FD_{idx}) will abnormally increase.

Based on a pre-determined threshold (PDT) value, which will be compared to the fault detection index, the open fault can be detected. The FD_{idx} value can increase for a short time period when the load suddenly increases, even though the load current (i_{LO}) is in the FD_{idx} equation as a part of the denominator. Therefore, both the pre-measured FD_{idx} and the change ratio (dFD_{idx}/dt) at a maximum load change have been used to detect the switch fault. The FD_{idx} change ratio has been calculated every 10 samples, which is during every 1 ms (sampling period is 100 μs). The fault detection index can reach to a threshold value (PDT) even under normal operations if there is an enormous load change. Therefore, the pre-measured change ratio (dFD_{idx}/dt) under normal operation with a maximum load change has been used to create a maximum value for normal operation. The maximum value has been used to distinguish between an open switch fault case and an enormous load change case.

Once the switch fault is detected based on the fault detection index, the system control activates a compensation control algorithm utilizing a mixed switching method explained in detail in the next sub-section.

B. FAULT COMPENSATION CONTROL METHOD

If an S_1 switch fault is detected, two other switches (S_a and S_b) need to operate based on modified switching statuses as shown in Figure 5 to boost the input voltage and to charge/discharge the battery at the same time.

1) FAULT COMPENSATION CONTROL FOR A CHARGING MODE

Based on the switching status in Figure 5, the inductor voltages (v_{L1} and v_{L2}), and the DC-bus capacitor current (i_{bus}) are summarized in Table 1 for a charging mode. For this summarization, voltage drops of switching devices and diodes are ignored for simplifications.

Based on Table 1, the main inductor average voltage, V_{L1}, at a steady state can be derived under the S_1 switch fault. As shown in (2), the average inductor voltage at a steady state is zero.

$$0 = v_{gen}\cdot D_{C2} + \left(v_{gen} - v_{bat} - v_{L2}\right)\cdot (D_{C1} - D_{C2}) + \left(v_{gen} - v_{bus}\right)\cdot (1 - D_{C1}) = V_{L1} \tag{2}$$

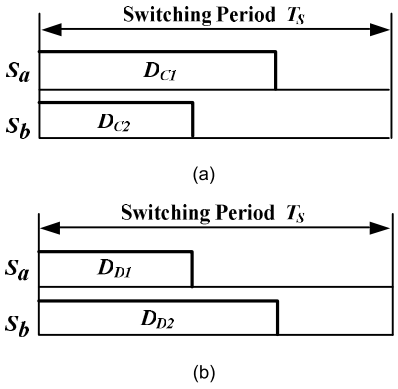

FIGURE 5. Switching statuses for charging and discharging modes with *S1* switch fault. (a) Battery charging mode. (b) Battery discharging mode.

Similarly, under the S_1 switch fault, the average voltage of the second inductor (V_{L2}) which is in the bi-directional dc-dc converter is calculated (at a steady state) based on Table 1 as,

$$0 = -v_{bat}\cdot D_{C2} + \left(v_{gen} - v_{bat} - v_{L1}\right)\cdot (D_{C1} - D_{C2}) + (-v_{bat})\cdot (1 - D_{C1}) = V_{L2} \tag{3}$$

In addition, the average DC-bus capacitor current, I_{bus}, is derived based on Table 1 as:

$$I_{bus} = -i_{LO}\cdot (D_{C2} + D_{C1} - D_{C2}) + (i_{L1} - i_{LO})\cdot (1 - D_{C1}) \tag{4}$$

Based on (2) $\sim$ (4), an inductor current for a charging mode under the switch fault is derived as:

$$i_{L1} = \frac{v_{bus}\cdot v_{gen}\cdot (I_{bus} + i_{LO})}{v^2_{gen} - v^2_{bat}} \tag{5}$$

Then, the inductor current command under the switch fault is formulated using the DC-bus voltage controller output (I^*_{bus}) and the equation (5) as:

$$i^*_{L1} = \frac{v_{bus}\cdot v_{gen}\cdot \left(I^*_{bus} + i_{LO}\right)}{v^2_{gen} - v^2_{bat}} \tag{6}$$

In a transient state, equations (2) and (3) will be modified using the outputs of the inductor current controllers (V^*_{L1}, V^*_{L2}) as:

$$V^*_{L1} = v_{gen}\cdot D_{C2} + \left(v_{gen} - v_{bat} - v_{L2}\right)\cdot (D_{C1} - D_{C2}) + (-v_{bat})\cdot (1 - D_{C1}) \tag{7}$$

$$V^*_{L2} = -v_{bat}\cdot D_{C2} + \left(v_{gen} - v_{bat} - v_{L1}\right)\cdot (D_{C1} - D_{C2}) + (-v_{bat})\cdot (1 - D_{C1}) \tag{8}$$

Then, desired duty ratios (D^*_{C1}, D^*_{C2}) under the switch fault are derived based on (7) and (8):

$$D^*_{C1} = \frac{V^*_{L1} - v_{gen} + v_{bus} + \delta\cdot \left(V^*_{L2} + v_{bat}\right)}{v_{bus}} \tag{9}$$

$$D^*_{C2} = D^*_{C1} - \delta \tag{10}$$

where,

$$\delta = \frac{V^*_{L2} + v_{bat}}{v_{gen} - V^*_{L1}} \tag{11}$$

TABLE 1. Status of v_{L1}, v_{L2}, and i_{bus} under S_1 switch fault (charging case).

Period & Status		v_{L1}	v_{L2}	i_{bus}
$D_{C2}\cdot T_S$	S_a=1 S_b=1	v_{gen}	$-v_{bat}$	$-i_{LO}$
$(D_{C1}-D_{C2})T_S$	S_a=1 S_b=0	$v_{gen}-v_{bat}$ $-v_{L2}$	$v_{gen}-v_{bat}$ $-v_{L1}$	$-i_{LO}$
$(1-D_{C1})T_S$	S_a=0 S_b=0	$v_{gen}-v_{bus}$	$-v_{bat}$	$i_{L1}-i_{LO}$

TABLE 2. Status of v_{L1}, v_{L2}, and i_{bus} under S_1 fault (discharging case).

Period & Status		v_{L1}	v_{L2}	i_{bus}
$D_{D1}\cdot T_S$	S_a=1 S_b=1	v_{gen}	$-v_{bat}$	$-i_{LO}$
$(D_{D2}-D_{D1})T_S$	S_a=0 S_b=1	$v_{gen}-v_{bus}$	$-v_{bat}$	$i_{L1}-i_{LO}$
$(1-D_{D2})T_S$	S_a=0 S_b=0	$v_{gen}-v_{bus}$	$v_{bus}-v_{bat}$	$i_{L1}-i_{L2}-i_{LO}$

2) FAULT COMPENSATION CONTROL FOR A DISCHARGING MODE

For a discharging mode, Table 2 will be used under the S_1 switch fault based on Figure 5(b).

For a discharging mode, the average inductor voltage, V_{L1}, at a steady state is as follows:

$$0=v_{gen}\cdot D_{D1}+\left(v_{gen}-v_{bus}\right)\cdot(D_{D2}-D_{D1}+1-D_{D2})=V_{L1} \quad (12)$$

The average voltage of the second inductor (V_{L2}) is:

$$0=-v_{bat}\cdot(D_{D1}+D_{D2}-D_{D1})+(v_{bus}-v_{bat})\cdot(1-D_{D2})=V_{L2} \quad (13)$$

The average DC-bus capacitor current is derived based on Table 2 as:

$$I_{bus}=-i_{LO}\cdot D_{D1}+(i_{L1}-i_{LO})\cdot(D_{D2}-D_{D1})+(i_{L1}-i_{L2}-i_{LO})\cdot(1-D_{D2}) \quad (14)$$

Based on (12)∼(14), an inductor current for a charging mode under a switch fault is derived as:

$$i_{L1}=\frac{v_{bus}\cdot(I_{bus}+i_{LO})+v_{bat}\cdot i_{L2}}{v_{gen}} \quad (15)$$

Then, the inductor current command for a discharging mode is formulated using the DC-bus voltage controller output (I^*_{bus}) and equation (15) as:

$$i^*_{L1}=\frac{v_{bus}\cdot\left(I^*_{bus}+i_{LO}\right)+v_{bat}\cdot i_{L2}}{v_{gen}} \quad (16)$$

Similar to the charging case, equations (12) and (13) will be modified using the outputs of the inductor current controllers (V^*_{L1}, V^*_{L2}) for a transient state,

$$V^*_{L1}=v_{gen}\cdot D_{D1}+\left(v_{gen}-v_{bus}\right)\cdot(D_{D2}-D_{D1}+1-D_{D2}) \quad (17)$$

$$V^*_{L2}=-v_{bat}\cdot(D_{D1}+D_{D2}-D_{D1})+(v_{bus}-v_{bat})\cdot(1-D_{D2}) \quad (18)$$

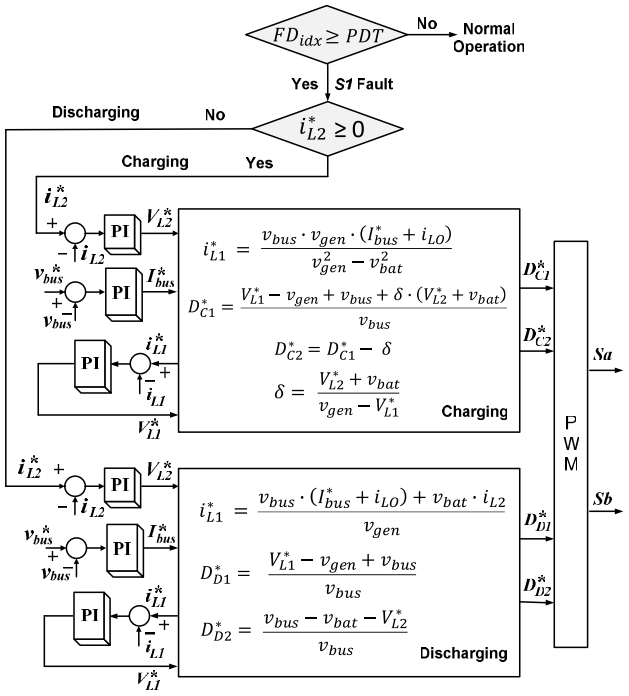

FIGURE 6. Compensation control structure under S_1 switch fault.

The duty ratios (D^*_{D1}, D^*_{D2}) under the switch fault are derived based on (17) and (18) for a discharging mode:

$$D^*_{D1}=\frac{V^*_{L1}-v_{gen}+v_{bus}}{v_{bus}} \quad (19)$$

$$D^*_{D2}=\frac{v_{bus}-v_{bat}-V^*_{L2}}{v_{bus}} \quad (20)$$

Figure 6 summarizes the compensation control scheme for both the charging and the discharging modes. Once the S_1 switch has an open switch fault, the output bus voltage will decrease. Then, the bus voltage controller will raise the inductor current command (i^*_{L1}). This will raise the fault detection index and at a certain point it will surpass the pre-determined threshold (PDT). At this moment, the S_1 switch fault is detected. By checking the battery current command (i^*_{L2}), the fault compensation algorithm will find a mode (either charging or discharging) as shown in Figure 6.

In each mode, the inductor current command (i^*_{L1}) is calculated first followed by the calculation of the duty ratios for the S_a and S_b switches.

In healthy conditions, the conventional control loops shown in Figure 4 are suitable to control the system. However, for fault compensation, the control structure based on mixed switching becomes sensitive to the load change, and hence the load current (i_{LO}) is used to derive an inductor current command (i^*_{L1}) based on the capacitor current command (I^*_{bus}), as shown in Figure 6. If the voltage controller output is a capacitor current command, the transfer function becomes a simple linear function and the control system is less sensitive to operating points [26].

TABLE 3. Converter circuit parameters.

Parameters	Value
Main inductor (*L1*)	2 [*mH*]
Second inductor (*L2*)	2 [*mH*]
DC-bus capacitor	470 [μF]
Switch (IGBT) max voltage	600 [V]
Switch (IGBT) max continuous current	30 [A]
Switching frequency	20 [kHz]

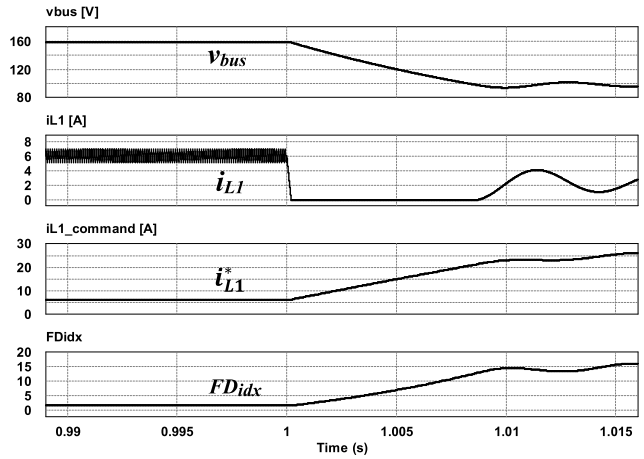

FIGURE 7. Simulation results: Converter response when S_1 switch open fault occurs. Top to bottom: DC-bus voltage (v_{bus}); main inductor current (i_{L1}); inductor current command (i^*_{L1}); fault detection index (FD_{idx}).

III. SIMULATION AND EXPERIMENTAL RESULTS

Based on the fault detection and compensation control schemes illustrated in Figure 6, simulations and experiments have been performed. Tables 3 specifies the converter circuit parameters.

Figure 7 shows simulation results of the circuit response when the S_1 switch open fault occurs. For this initial simulation, a resistive load is connected (40 Ω). The inductor current i_{L1} will decrease and become zero until the bus voltage falls below the input voltage. Once the DC bus voltage becomes lower than the input voltage, the input source delivers power to the output side again and hence the inductor current flows again as presented in Figure 7. In this situation, the voltage controller will abnormally increase the inductor current command (i^*_{L1}) until it reaches to a current limit as presented in Figure 7. The S_1 switch fault detection relies on the fault detection index (FD_{idx}) as indicated in (1). To control the output voltage (v_{bus}), the boost converter controller increases the inductor current command and hence the fault detection index (FD_{idx}) will soar.

The fault detection index starts to rise when an open switch fault occurs at $t = 1$ sec. Based on a PDT value, which will be compared to the fault detection index. the open fault can be detected. Figure 8 shows the proposed fault compensation approach based on the FD_{idx} signal. Once the switch fault is detected, the fault compensation method with the S_a and S_b switches is applied to boost the DC bus voltage while at

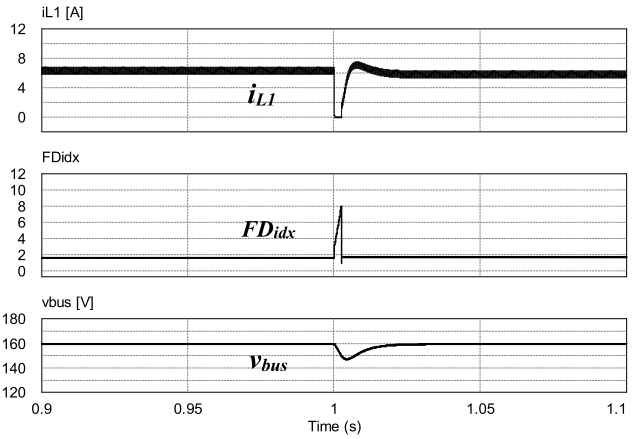

FIGURE 8. Simulation results: Converter response based on the fault compensation scheme. Top to bottom: Main inductor current (i_{L1}); fault detection index (FD_{idx}); DC-bus voltage (v_{bus}).

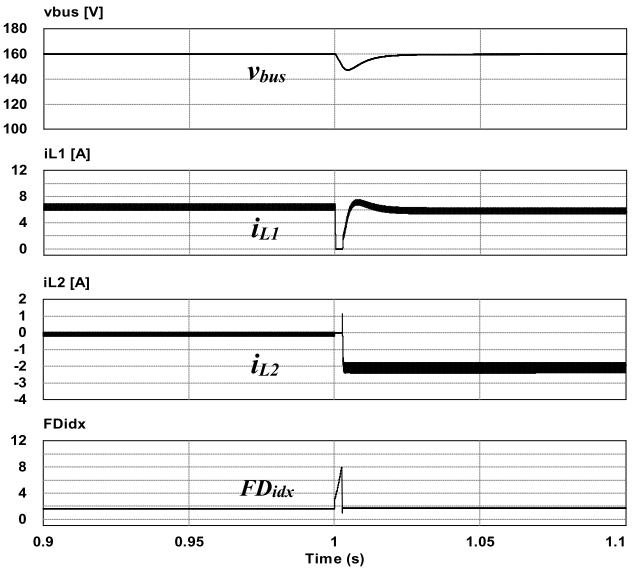

FIGURE 9. Simulation results: Fault compensation using the battery discharging.Top to bottom: DC-bus voltage (v_{bus}); main inductor current (i_{L1}); second inductor current (i_{L2}); fault detection index (FD_{idx}).

the same time managing the energy storage using the compensation control shown in Figure 6. The system response of the fault detection and the compensation control is presented in Figure 8. The DC bus voltage is reverted to 160 V based on the compensation.

In addition to the fault compensation method, the battery can be used for faster voltage recovery. The system controller can create a discharging current command while the compensation control is applied. As shown in Figure 9, for a faster voltage recovery, the battery supplies a current right after the fault detection.

This battery discharging can support to increase the fallen DC bus voltage after the fault occurrence. In Figure 9, i_{L2} current indicates the battery discharging (0A → -2A) to

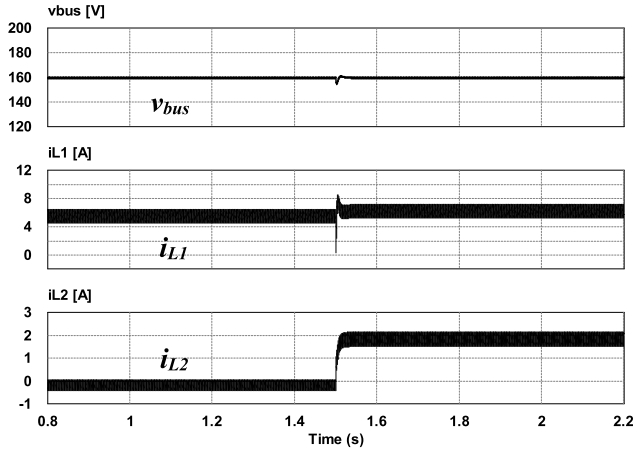

FIGURE 10. Simulation results: A system response under a step charging current command change with the fault compensation control after the S_1 switch fault occurrence. Top to bottom: DC-bus voltage (v_{bus}); main inductor current (i_{L1}); second inductor current (i_{L2}).

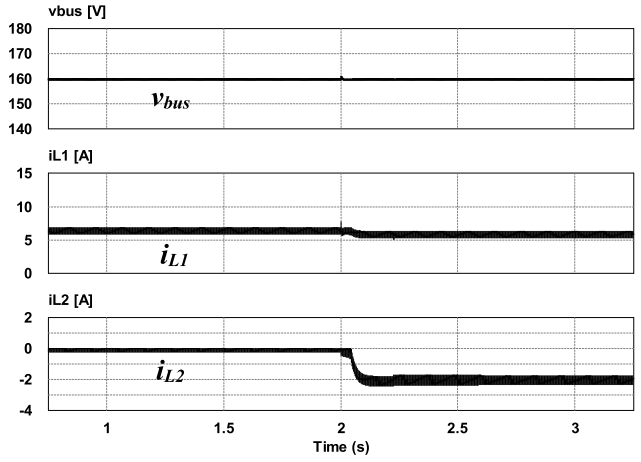

FIGURE 11. Simulation results: A step current (battery discharging) response based on the fault tolerant converter under S_1 switch fault. Top to bottom: DC-bus voltage (v_{bus}); main inductor current (i_{L1}); second inductor current (i_{L2}).

support the fault compensation control for a faster DC bus voltage recovery.

Figures 10 and 11 present the fault-tolerant converter's performance based on the compensation algorithm shown in Figure 6. In this case, a resistor is used as a load instead of an inverter and an AC load. Figure 10 presents a step charging-current response while the DC-bus voltage is being regulated under the S_1 switch fault. In addition, Figure 11 shows a step-discharging-current response. These tests assure that the compensation control algorithm can still control the bus voltage and battery charging/discharging simultaneously under the S_1 switch fault.

Figure 12 presents simulation results of the fault compensation scheme with a single-phase inverter and a RL (40 Ω resistor and 10 mH inductor) load based on a constant DC source. The fault detection and compensation methods

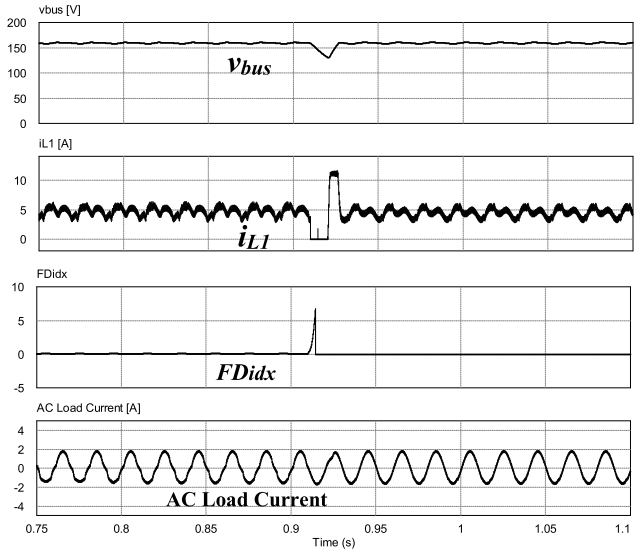

FIGURE 12. Simulation results: Fault detection and compensation with a single-phase AC inverter. Top to bottom: DC bus voltage (v_{bus}); Inductor current (i_{L1}); fault detection index (FD_{idx}); AC load current.

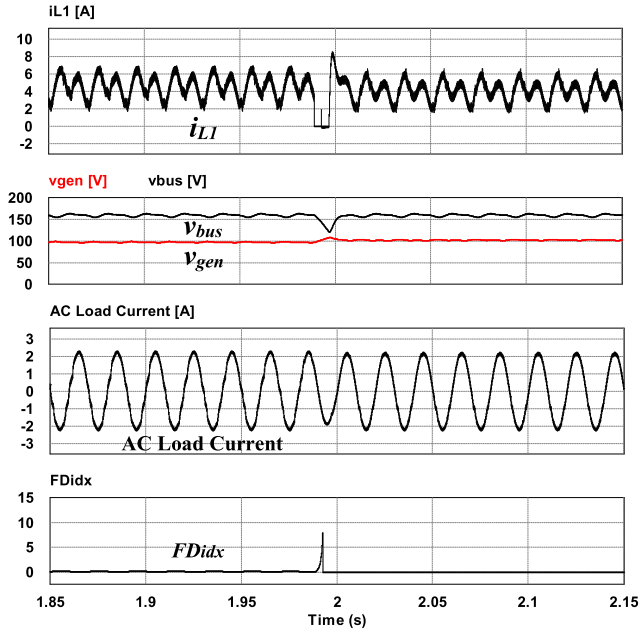

FIGURE 13. Simulation results: Fault detection and compensation using a wind turbine model. Top to bottom: Inductor current (i_{L1}); DC bus voltage (v_{bus}) and generated DC voltage (v_{gen}); AC load current; fault detection index (FD_{idx}).

minimize the DC-bus voltage sag to maintain the AC output voltage under the S_1 switch fault.

Figure 13 shows simulation results with a wind turbine model, which has a PMSM synchronous generator and a three-phase rectifier. One of the waveforms in the second screen presents a generated DC voltage (v_{gen} in Figure 2), which is an output of the rectifier circuit. Right after an open-circuit fault, the v_{gen}voltage increases for a short period before the compensation algorithm kicks in, since the input

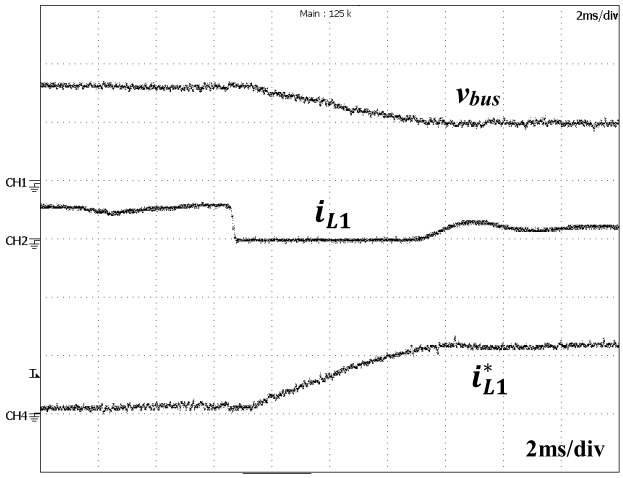

FIGURE 14. Experimental results: Circuit behavior when the S_1 switch fault occurs. Top to bottom: V_{bus} voltage (100 V/div); Inductor current, i_{L1} (10 A/div); Inductor current command, i^*_{L1} (25 A/div).

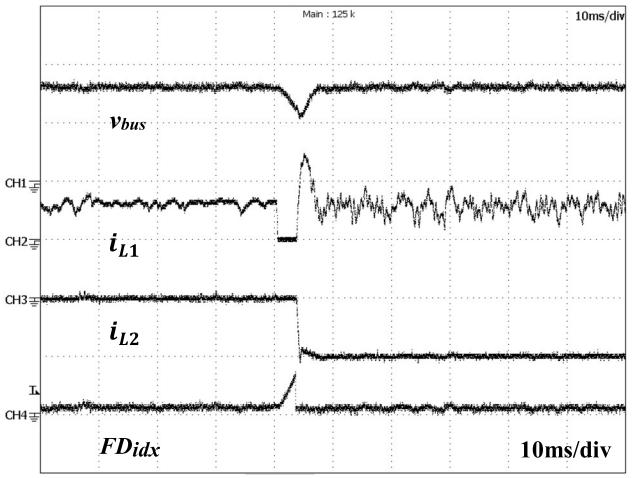

FIGURE 15. Experimental results: Fault detection and compensation procedure. Top to bottom: v_{bus} voltage (100 V/div); i_{L1} current (5 A/div); i_{L2} current (2 A/div); fault detection index, FD_{idx} (10/div).

power is not delivered to the output side (the generator load is suddenly reduced).

The results indicate that the fault detection and compensation mechanism is similar to the case in Figure 12, which used a constant DC source (100 V) as an input.

Figures 14∼18 present experimental results. The converter circuit behavior when an open fault occurs in the S_1 switch without fault compensation is presented in Figure 14. The output bus voltage (v_{bus}) falls down to the input voltage, and the current command of the main inductor (i^*_{L1}), which is the output of the voltage controller, keeps on increasing until it reaches a predetermined current limit.

Based on the observation indicated in Figure 14, the proposed fault compensation control is implemented in the Texas Instruments' TMS320F28335 DSP and the result is presented in Figure 15. An internal digital-to-analog (D/A) converter in the DSP has been used to display the calculated fault detection index (FD_{idx}). Similar to the simulation results shown in Figure 9, the index rises rapidly after the switch fault occurrence.

The proposed fault compensation approach is immediately applied right after the fault detection using the FD_{idx} signal.

Figure 16 presents the fault compensation with a single-phase inverter. The fault detection and compensation schemes are applied to minimize the DC-bus voltage sag. Due to the fast fault detection and compensation, the inverter output current is not influenced much by the switch fault.

Figure 17 shows a step current (battery charging current) response with the fault tolerant control strategy under the S_1 switch fault. The output DC-bus voltage is being regulated at 160 V and the battery charging current is step changed to observe the system response.

Figure 18 presents a discharging current response to follow a step current command under the S_1 switch fault. Figures 17 and 18 both show that the fault-tolerant converter

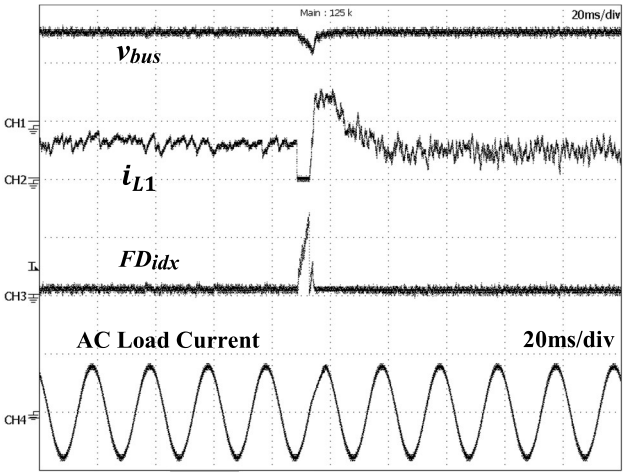

FIGURE 16. Experimental results: Fault detection and compensation with a single-phase AC inverter. Top to bottom: v_{bus} voltage (100 V/div); Inductor current, i_{L1}, (10 A/div); fault detection index, FD_{idx} (5/div); AC load current (3 A/div).

and control algorithm can manage both the DC-bus voltage and battery charging/discharging current reasonably well.

Figure 19 shows the measured efficiency comparison between the normal operation with all three switches and the fault tolerant operation with two switches (when S_1 switch open fault occurred). Since the system lost the S_1 switch, it has less total switching losses during the fault tolerant operation than the normal operation case which uses all three switches.

This influences the system efficiency having slightly better efficiency when the system is operating under the fault tolerant control without the S_1 switch as shown in Figure 19.

For normal operation, the power conversion system structure operates in the same way as the conventional structure. However, under open switch fault, the S_a and S_b switches are operating for two control purposes and the switching

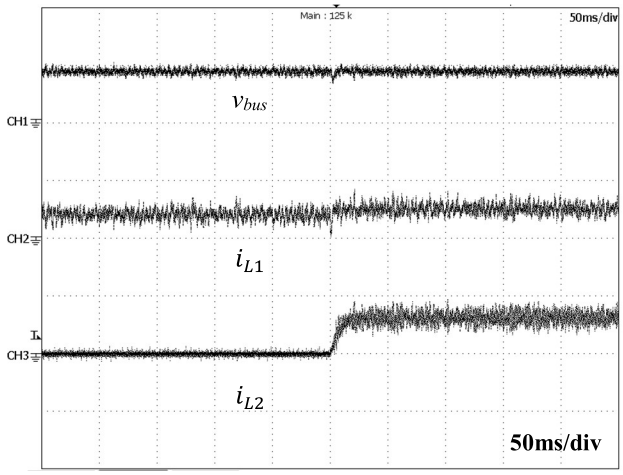

FIGURE 17. Experimental results: A step current (charging current) response of the fault tolerant converter under S_1 switch fault. Top to bottom: v_{bus} voltage (200 V/div); Inductor current, i_{L1}, (10 A/div); battery current, i_{L2}, (3 A/div).

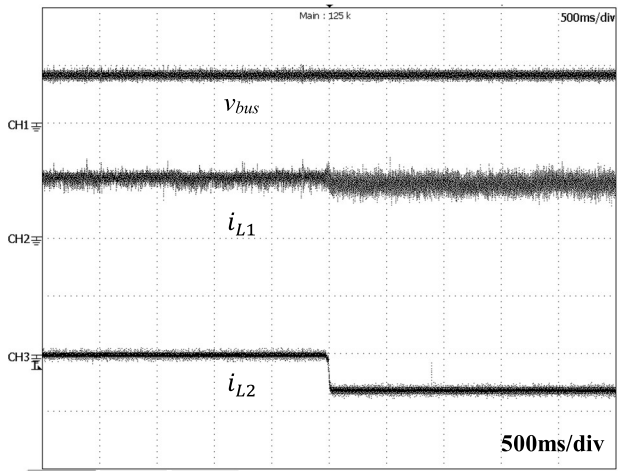

FIGURE 18. Experimental result: A step current (discharging current) response of the fault tolerant converter. Top to bottom: V_{bus} voltage (200 V/div), Inductor current, i_{L1}, (10 A/div), battery current, i_{L2}, (3 A/div).

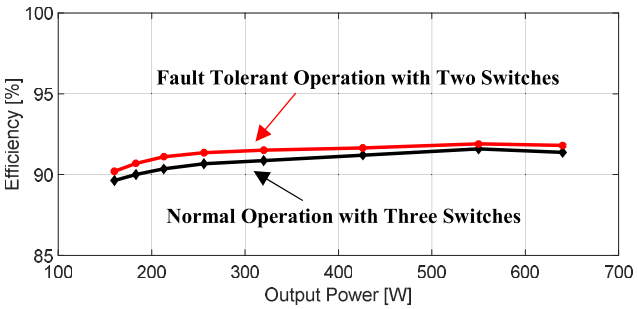

FIGURE 19. Measured efficiency comparison between the normal operation with three switches (S_1, *Sa*, *Sb*) and the fault tolerant operation (with *Sa* and *Sb*, lost S_1).

period is not fully utilized for a single control purpose. Since the switching period is shared for two control purposes under open faults, a decrease in maximum possible load is not avoidable. To accommodate the two control purposes, the maximum possible output load under the open fault is limited to 80% of the maximum power under normal operation (without switch faults) to maintain the voltage boosting capability.

Overall, Figures. 14∼19 assure that the proposed fault detection and compensation control methods can make the system continue to operate while not sacrificing performance much under the S_1 switch fault

IV. CONCLUSION

In this paper, an open switch fault detection strategy and a compensation method have been proposed for a modified dc-dc converter for alternative energy harvesting systems. The compensation controller utilizes two switches in the energy storage management circuits to make the system keep on operating under a switch fault in the modified boost converter. A fault detection index has been developed to detect switch faults as quickly as possible. Under a switch fault, the proposed fault compensation algorithm can manage both the boosting operation and the charging/discharging of an energy storage device based on a mixed switching strategy. The simulation and experimental results validate the proposed concept and control strategy.

REFERENCES

[1] F. Blaabjerg, Y. Yang, D. Yang, and X. Wang, "Distributed power-generation systems and protection," *Proc. IEEE*, vol. 105, no. 7, pp. 1311–1331, Jul. 2017.

[2] V. Yaramasu, B. Wu, P. C. Sen, S. Kouro, and M. Narimani, "High-power wind energy conversion systems: State-of-the-art and emerging technologies," *Proc. IEEE*, vol. 103, no. 5, pp. 740–788, May 2015.

[3] M. D. P. Gil, J. L. Domínguez-García, F. Díaz-González, M. Aragüés-Peñalba, and O. Gomis-Bellmunt, "Feasibility analysis of offshore wind power plants with DC collection grid," *Renew. Energy*, vol. 78, pp. 467–477, Jun. 2015.

[4] F. Blaabjerg and K. Ma, "Future on power electronics for wind turbine systems," *IEEE J. Emerg. Sel. Topics Power Electron.*, vol. 1, no. 3, pp. 139–152, Sep. 2013.

[5] F. Blaabjerg and Z. Chen, "Power electronics as an enabling technology for renewable energy integration," *J. Power Electron.*, vol. 3, no. 2, pp. 81–89, Apr. 2003.

[6] K. Musasa, N. I. Nwulu, M. N. Gitau, and R. C. Bansal, "Review on DC collection grids for offshore wind farms with high-voltage DC transmission system," *IET Power Electron.*, vol. 10, no. 15, pp. 2104–2115, Dec. 2017.

[7] A. D. Hansen, F. Iov, F. Blaabjerg, and L. H. Hansen, "Review of contemporary wind turbine concepts and their market penetration," *Wind Eng.*, vol. 28, no. 3, pp. 247–263, 2004.

[8] Y. Yang, P. Enjeti, F. Blaabjerg, and H. Wang, "Wide-scale adoption of photovoltaic energy: Grid code modifications are explored in the distribution grid," *IEEE Ind. Appl. Mag.*, vol. 21, no. 5, pp. 21–31, Sep./Oct. 2015.

[9] T. Park and T. Kim, "Novel energy conversion system based on a multi-mode single-leg power converter," *IEEE Trans. Power Electron.*, vol. 28, no. 1, pp. 213–220, Jan. 2013.

[10] M. Jang, M. Ciobotaru, and V. G. Agelidis, "A single-phase grid-connected fuel cell system based on a boost-inverter," *IEEE Trans. Power Electron.*, vol. 28, no. 1, pp. 279–288, Jan. 2013.

[11] E. N. Hinrichsen, "Controls for variable pitch wind turbine generators," *IEEE Trans. Power App. Syst.*, vol. 103, no. 4, pp. 886–892, Apr. 1984.

[12] K. Kobayashi, H. Matsuo, and Y. Sekine, "Novel solar-cell power supply system using a multiple-input DC-DC converter," *IEEE Trans. Ind. Electron.*, vol. 53, no. 1, pp. 281–286, Feb. 2006.

[13] T. Kim and S. Kwak, "Single pole switch leg based multi-port converter with an energy storage," *IET Power Electron.*, vol. 9, no. 6, pp. 1322–1330, May 2016.

[14] R.-J. Wai and R.-Y. Duan, "High-efficiency power conversion for low power fuel cell generation system," *IEEE Trans. Power Electron.*, vol. 20, no. 4, pp. 847–856, Jul. 2005.
[15] T. Kim and S. Baek, "Switch fault detection and compensation technique in a boost DC-DC converter for renewable energy generation systems," in *Proc. 9th IEEE Int. Symp. Power Electron. Distrib. Gener. Syst.*, Jun. 2018, pp. 1–6.
[16] Z. Gao, C. Cecati, and S. X. Ding, "A survey of fault diagnosis and fault-tolerant techniques-Part I: Fault diagnosis with model-based and signal-based approaches," *IEEE Trans. Ind. Electron.*, vol. 62, no. 6, pp. 3757–3767, Jun. 2015.
[17] Y. Chen, X. Pei, S. Nie, and Y. Kang, "Monitoring and diagnosis for the DC-DC converter using the magnetic near field waveform," *IEEE Trans. Ind. Electron.*, vol. 58, no. 5, pp. 1634–1647, May 2011.
[18] M. Shahbazi, E. Jamshidpour, P. Poure, S. Saadate, and M. R. Zolghadri, "Open-and short-circuit switch fault diagnosis for nonisolated DC-DC converters using field programmable gate array," *IEEE Trans. Ind. Electron.*, vol. 60, no. 9, pp. 4136–4146, Sep. 2012.
[19] H. Givi, E. Farjah, and T. Ghanbari, "Switch and diode fault diagnosis in nonisolated DC-DC converters using diode voltage signature," *IEEE Trans. Ind. Electron.*, vol. 65, no. 2, pp. 1606–1615, Feb. 2018.
[20] A. Izadian and P. Khayyer, "Application of Kalman filters in model-based fault diagnosis of a DC-DC boost converter," in *Proc. 36th Annu. Conf. IEEE Ind. Electron. Soc.*, Glendale, AZ, USA, Nov. 2010, pp. 369–372.
[21] E. Ribeiro, A. J. M. Cardoso, and C. Boccaletti, "Open-circuit fault diagnosis in interleaved DC-DC converters," *IEEE Trans. Power Electron.*, vol. 29, no. 6, pp. 3091–3102, Jun. 2014.
[22] E. Pazouki, Y. Sozer, and J. A. D. Abreu-Garcia, "Fault diagnosis and fault-tolerant control operation of nonisolated DC-DC converters," *IEEE Trans. Ind. Appl.*, vol. 54, no. 1, pp. 310–320, Feb. 2018.
[23] E. Ribeiro, A. J. M. Cardoso, and C. Boccaletti, "Fault-tolerant strategy for a photovoltaic DC–DC converter," *IEEE Trans. Power Electron.*, vol. 28, no. 6, pp. 3008–3018, Jun. 2013.
[24] E. Jamshidpour, P. Poure, and S. Saadate, "Photovoltaic systems reliability improvement by real-time FPGA-based switch failure diagnosis and fault-tolerant DC-DC converter," *IEEE Trans. Ind. Electron.*, vol. 62, no. 11, pp. 7247–7255, Nov. 2015.
[25] *Constant Voltage, Constant Current Battery Charging*. Accessed: Sep. 1, 2018. [Online]. Available: http://power-topics.blogspot.com/2016/05/constant-volta-ge-constant-current.html
[26] K.-W. Lee and T. Kim, "Operating-point insensitive voltage control of the Z-source inverter based on an indirect capacitor current control," *IET Power Electron.*, vol. 8, pp. 1358–1366, Apr. 2015.

TAEHYUNG KIM (M'04–SM'12) received the Ph.D. degree in electrical engineering from Texas A&M University, College Station, TX, USA, in 2003. He was with Samsung Electronics' Digital Appliances Research Center as a Senior Research Engineer, in 2003. From 2004 to 2005, he was a Postdoctoral Researcher with the Advanced Vehicle, Power Electronics, and Motor Drive Laboratory, Texas A&M University. In 2005, he joined the Department of Electrical and Computer Engineering, University of Michigan-Dearborn, where he is currently an Associate Professor. In 2014, he visited Chung-Ang University as an invited Brain-Pool Research Scholar. His research interests include electric and hybrid electric vehicles, power electronics, and motor drives. He was a recipient of the 2012 Second Prize Paper Award from the IEEE Industry Applications Society (Annual Society's Best Magazine Article).

HYUNG-WOO LEE (M'98) received the M.S. degree from Hanyang University, Seoul, South Korea, in 2000, and the Ph.D. degree from Texas A&M University, College Station, TX, USA, in 2003, both in electrical engineering. He was a Postdoctoral Research Assistant with the Department of Theoretical and Applied Mechanics, Cornell University, Ithaca, NY, USA, in 2004. He was with the Korea Railroad Research Institute as a Senior Researcher, from 2006 to 2013. He joined the Korea National University of Transportation as an Associate Professor with the Department of Railway Vehicle System Engineering, in 2013. His current research interests include design, analysis, and control of the motor/generator, power conversion systems, and applications of motor drives such as Maglev trains, conventional railway propulsion systems, and modern renewable energy systems.

SANGSHIN KWAK (M'05) received the Ph.D. degree in electrical engineering from Texas A&M University, College Station, TX, USA, in 2005. From 1999 to 2000, he was a Research Engineer with LG Electronics, Changwon, South Korea. He was also with Whirlpool R&D Center, Benton Harbor, MI, USA, in 2004. From 2005 to 2007, he was a Senior Engineer with the Samsung SDI R&D Center, Yongin, South Korea. From 2007 to 2010, he was an Assistant Professor with Daegu University, Gyeongsan, South Korea. Since 2010, he has been with Chung-Ang University, Seoul, South Korea, where he is currently a Professor. His research interests are topology design, modeling, modulation, and control of power converters, multilevel converters, renewable energy systems, and power quality.